Available online at www.sciencedirect.com
SCIENCE DIRECT®
International Journal of Heat and Mass Transfer 48 (2005) 3604–3614
International Journal of HEAT and MASS TRANSFER
www.elsevier.com/locate/ijhmt

Soot graphitic order in laminar diffusion flames and a large-scale JP-8 pool fire

Christopher R. Shaddix [a,*], Árpád B. Palotás [b], Constantine M. Megaridis [c], Mun Y. Choi [d], Nancy Y.C. Yang [e]

[a] Combustion Research Facility, Sandia National Laboratories, MS 9052, 7011 East Avenue, Livermore, CA 94550, United States
[b] Department of Combustion Technology, University of Miskolc, H-3515 Miskolc-Egyetemvaros, Hungary
[c] Department of Mechanical and Industrial Engineering, University of Illinois at Chicago, Chicago, IL 60607, United States
[d] Department of Mechanical Engineering and Mechanics, Drexel University, Philadelphia, PA 19104, United States
[e] Analytical Materials Science Department, Sandia National Laboratories, Livermore, CA 94550, United States

Received 22 October 2004; received in revised form 2 March 2005
Available online 17 May 2005

Abstract

High-resolution transmission electron microscopy (HRTEM) has been performed on soot samples collected from two smoking laminar ethylene diffusion flames (one steady and one unsteady) and from the active-flaming region of a 5-m diameter JP-8 pool fire. The motivation for this study is to improve the understanding of the influence of soot microstructure on its optical properties. The soot sampling positions in the steady ethylene flame correspond to locations of maximum soot mass growth, partial soot oxidation, and quenched oxidation along a common streamline. Visual examination of the HRTEM images suggests that the graphitic crystalline layers of soot undergo increased densification along the sampled streamline in the steady laminar flame. Quantitative image analysis reveals a small decrease in the mean graphitic interlayer spacing (d_{002}) with increasing residence time in the high-temperature region. However, the differences in the mean interlayer spacing are far smaller than the spread of interlayer spacings measured for any given soot sample. Post-flame samples from the unsteady ethylene flame show interlayer spacing distributions similar to the lower region of the steady flame. The soot samples from the pool fire show little evidence of oxidized soot and have interlayer spacings similar to the unsteady ethylene flame. Previous research in the carbon black field has demonstrated a direct relation between the graphitic interlayer spacing and the optical absorptivity of the carbon. Consequently, the current HRTEM results offer support to recent measurements of the dimensionless extinction coefficient of soot that suggest that the optical absorptivity of agglomerating soot shows only minor variations for different fuels and flame types.

Keywords: Soot; HRTEM; Diffusion flame; Pool fire; Interlayer spacing; Optical properties

* Corresponding author. Tel.: +1 925 294 3840; fax: +1 925 294 2276.
E-mail address: crshadd@sandia.gov (C.R. Shaddix).

0017-9310/$ - see front matter © 2005 Elsevier Ltd. All rights reserved.
doi:10.1016/j.ijheatmasstransfer.2005.03.006

Nomenclature

D_f	fractal dimension	n	dispersion exponent
d_p	soot primary particle diameter	N_p	number of primary particles in a soot aggregate
d_{002}	interlayer atomic spacing between two parallel aromatic carbon layers	R_g	radius of gyration of agglomerate
C	constant of proportionality	sp^2	bonding state involving one unfilled s orbital and 2 unfilled p orbitals
f_v	soot volume fraction	sp^3	bonding state involving one unfilled s orbital and 3 unfilled p orbitals
H	height above the burner surface	x_p	non-dimensional size parameter
I	transmitted light intensity	λ	wavelength of light
I_0	incident light intensity		
k_f	mass fractal pre-factor term		
L	optical pathlength		

1. Introduction

Several investigations of the fine structure of combustion-generated soot have been recently reported, yielding insight into the formation mechanism of soot [1,2], the source of ambient soot [3], the effect of intermediate-temperature oxidation on the internal structure of soot [4], and the effect of residence time on the development of fullerenic carbon [5–8]. These studies have all relied upon high-resolution transmission electron microscopy (HRTEM) as the primary diagnostic for soot nanostructure. Chen and Dobbins [2] also utilized X-ray diffraction (XRD) and dark field transmission electron microscopy (DFTEM) to provide complementary information. The interpretation of HRTEM imaging of carbon forms has become semi-automated and fairly quantitative over the past decade, through the development of advanced filtered image analysis routines that can evaluate carbon lattice fringes for parameters such as circularity, elongation, fringe length, fringe orientation, interplanar spacing (d_{002}), and fractional pattern coverage [9–12]. These improvements in the analysis of HRTEM have made it a very useful tool for evaluating changes in soot nanostructure, especially because standard analytical techniques such as XRD, ^{13}C nuclear magnetic resonance (NMR), and Raman spectroscopy require significant amounts of sample material. In fact, XRD and Raman are inherently ill-suited for analysis of soot because soot has a paracrystalline structure, with bent graphene layers that are concentrically arranged around one or more amorphous growth centers [13], and these measurement techniques are best suited for interrogation of carbon forms with planar ordered structures.

The current investigation is motivated by the desire to determine the extent of thermal annealing of soot during its natural thermal and chemical evolution in both laminar and fully turbulent buoyant, smoking diffusion flames, and, from these results, to gauge the extent of variation in soot optical absorptivity in these flame systems. This latter goal has the important, practical consequence of providing guidance for the choice of soot optical properties that are appropriate to use in interpreting optical and laser-based measurements of soot concentrations and temperature, and in predicting radiant heat transfer from these flames. The soot nanostructure also affects the reactivity of the soot particles, both for surface growth and oxidation. However, soot particle reactivity is predominately a surface phenomenon and therefore cannot be treated as rigorously via HRTEM analysis as volumetric (i.e., Rayleigh-limit) optical absorption, and will not be considered further here. Before describing the details of the current investigation, a brief review is included of the state of knowledge of soot optical properties and their relation to soot microstructure, temperature, and chemistry. This background is required for a proper appreciation of the motivation for this study and for a full understanding of the implications of the results.

1.1. Optical properties of soot aggregates

Considerable effort over the past decade has been spent characterizing the light scattering properties of aggregated primary soot particles, specifically using fractal aggregate approaches. Sorensen [14] recently reviewed these approaches and their regions of applicability. It appears that the relatively simple Rayleigh–Debye–Gans polydisperse fractal aggregate (RDG/PFA) theory, which ignores internal multiple scattering, can accurately describe the angle-dependent light scattering from aggregated soot particles, as long as the fractal dimension, D_f, used in the mass fractal analysis [15]

$$N = k_f \left(\frac{R_g}{d_p}\right)^{D_f}$$

is less than 2. In the above formulation, k_f is the fractal prefactor, R_g is the agglomerate radius of gyration, and d_p is the primary particle diameter. This condition is generally satisfied, because soot tends to form

diffusion-limited cluster aggregates with a $D_f \sim 1.8$ [14,16–21]. The RDG/PFA theory inherently assumes that the absorption coefficient of soot is independent of the extent of aggregation and depends solely on the refractive index of the soot and its volume fraction in the flow.

Calculations of soot aggregate scattering and absorption properties have also been performed using a coupled magnetic and electric dipole method, which includes the effects of internal multiple scattering [22,23]. These calculations have shown that for relatively small soot primary particle sizes (i.e., for the non-dimensional size parameter $x_p < 0.3$, where $x_p = \pi d_p/\lambda$) the soot absorptivity is ~10% higher than the RDG predictions for both small and large aggregates, because of enhanced fields at each primary particle from the multiple scattering. For larger primary particles ($x_p > 0.6$), shielding effects eventually dominate over the enhancement effect from multiple scattering and can result in up to a 30% decrease in absorptivity for large aggregates ($N_p \sim 1000$) [23]. The contribution of scattered light to the overall extinction from soot varies strongly with soot primary particle size and aggregate size, until a saturation regime is reached for large aggregates. For $x_p \sim 0.2$ (a typical value for soot illuminated by a visible light source), coupled dipole calculations and experimental measurements both show that scattering contributes approximately 20–30% of the total light extinction for large agglomerates [23–26].

1.2. Temperature dependence of soot optical properties

The understanding of the dependence of soot optical properties on temperature is much poorer than the understanding of its dependence on aggregate structure. By temperature dependence, in this context, we are referring to the dependence of the optical properties at any given wavelength as a function of soot temperature, on account of changes in the chemical bonding of the material. Obviously, the total emissivity and absorptivity of soot will change with temperature because of variations in the spectral absorptivity of soot and the varying blackbody spectral distribution with temperature. A limited number of studies over the years have tried to resolve the temperature dependence of soot optical properties, with limited success. Becker [27] and later Millikan [28] observed that values of the dispersion exponent, n, derived from visible light extinction measurements, were unchanged for soot when measured in situ in a flame or when measured for soot collected from the same flame location with a cooled plate. The dispersion exponent is derived from fits to spectral variation in light extinction of the form $\ln(I_0/I) = Cf_v L/\lambda^n$. Whereas the results from Becker and Millikan are not definitive evidence for invariance of all soot optical properties with temperature, they are suggestive of such invariance. Lee and Tien [29] and Charalampopoulos et al. [30] calculated the temperature dependence of the index of refraction of soot, assuming that the Drude–Lorentz dispersion model holds for soot, with the same resonant frequencies as graphite and with the assumption that the damping constants are proportional to the square root of the absolute temperature. With these assumptions, the real part of the refractive index is insensitive (<5% variation at visible wavelengths) to the soot temperature, whereas the imaginary part (associated with optical absorption) varies by up to 50% from room temperature up to flame temperatures. Stagg and Charalampopoulos [31] performed the only reported direct experimental determination of the index of refraction of soot, along with amorphous carbon and pyrolytic graphite, as a function of temperature, employing ellipsometry on samples contained within a furnace. For all 3 carbonaceous materials, the index of refraction showed negligible variation at visible wavelengths over the range of temperatures investigated (25–600 °C), in marked contrast to the earlier predictions with the dispersion model. Stagg and Charalampopoulos noted, however, that there are reasons to expect the temperature dependence of the optical properties to be stronger at infrared wavelengths.

1.3. Soot chemistry and optical properties

The effect of soot chemistry on its optical properties has been highlighted over the past decade with the revelation of the apparently common, if not universal, appearance of fairly transparent, liquid-like soot "precursor particles" in the soot inception region of both premixed and diffusion flames [1]. As these particles are heated, they undergo dehydrogenation, solidify, and become the broadband-absorbing (i.e., black) particles that have been traditionally recognized as normal, or "mature" soot [32]. Unlike the precursor particles, the mature soot particles do not coalesce upon collision with one another, but rather agglomerate into the wispy chains generally found in sooting flames. Wersborg et al. [33] made an early measurement of the absorption coefficient of precursor particles in a low-pressure premixed flame and found the optical absorptivity to be over an order of magnitude lower than that of mature soot. Millikan [28], Bonne and Wagner [34], and D'Alessio et al. [35] performed extinction scans in sooting premixed flames with broadband lamp sources and monochromator detection, allowing the fit of dispersion exponents. In all cases, the dispersion exponent was found to decrease uniformly with height above the burner. Millikan and D'Alessio et al. plotted the dispersion exponent against the molar H/C ratio in collected soot and found similar, approximately linear relationships, with incipient soot having an H/C ratio of 0.5–0.6 and a dispersion exponent of ~2.0. As the H/C ratio in the soot decreased

to values of ~0.2 (with either increasing height above the burner or for different flame chemistries), the dispersion exponent decreased to ~1.2. Dobbins and coworkers [1,32,36] have characterized precursor particles as having a molar H/C ratio between approximately 0.25–0.6, whereas solid, carbonaceous soot generally has an H/C ratio less than 0.20. Therefore, it appears that the earlier referenced studies of dispersion exponent variation primarily were focused on precursor particles, where strong variation in the optical properties with increasing dehydrogenation is expected. Indeed, Minutolo et al. [37] have presented an elegant analysis of the evolution of absorption spectra in a near-sooting premixed flame in which the extension of the absorption band from the UV to the visible (and ultimately into the infrared) of the large aromatic hydrocarbons and precursor particles is associated with the decreasing magnitude of the Tauc band gap (referring to the energy separation between valence electrons and conduction electrons) as the aromatic clusters grow in size within the particles. Indeed, the band gap energy appears to correlate linearly with the optical extinction dispersion coefficient and with the precursor material H/C ratio.

The connection between the chemical structure of carbonaceous material and its electrical and optical properties has been explored by researchers in the carbon black, astrophysics, and fullerene formation communities, where this issue is of vital importance. On a local, mesoscale level, a distinction is made between amorphous carbon, characterized by sp^3 hybridized carbon, and graphitic carbon, characterized by sp^2 hybridized carbon. Diamond and methane both contain carbon with sp^3 bonding, with the four valence electrons assigned tetrahedrally to form strong, isotropic σ bonds with the adjacent atoms. This type of bonding produces carbon that is quite transparent to visible and infrared radiation and which has high electrical resistivity. Benzene is an example of sp^2 bonded carbon, where 3 of the valence electrons are directed trigonally to form σ bonds in the plane, and the 4th valence electron forms a weak π bond perpendicular to the σ bonding plane. Consequently, graphitic carbon is highly anisotropic, having optical transparency and electrical resistivity in its axial direction and strong optical absorptivity and electrical conductivity perpendicular to its axis. The sp^2 hybridized carbon tends to form planar graphitic microcrystallites embedded in an amorphous structure. The bent, paracrystalline graphene layer ordering that is present in furnace black and in soot results from the incorporation of some sp^3 bonded carbon in the sp^2 bonded layers, producing a mixed hybridization state [13]. Various effective medium approaches have been proposed for calculating optical properties of carbon material that is a mixture of amorphous (sp^3) and graphitic (sp^2) phases, where the anisotropy of the graphitic phase adds complications [13,38–40].

2. Experimental methods

Soot samples from three different flames were interrogated in this study, as shown in Table 1. For the laminar flames, TEM grid samples were collected using a rapid-injection, short-hold thermophoretic sampling technique with the grids oriented vertically [41]. Copper grids with a lacey carbon film were utilized, to avoid interference during the TEM analysis from the amorphous carbon film that is more typically used for TEM sampling. For the pool fire, the soot samples were collected with carbon film grids oriented horizontally and exposed for 0.3 s [42].

Flame 1 is a 1.1-cm diameter smoking ethylene flame with forced co-annular air flow and was operated under conditions matching the steady "smoking" or "S" ethylene diffusion flame that has been extensively studied by Santoro and coworkers [43–45] and by Megaridis and Dobbins [41,46]. The cold-flow, area-averaged exit velocity was 5.07 cm/s for ethylene and 16.2 cm/s for air. Because the flame tip is open and emits smoke, the luminous flame height is poorly defined for this flame, but is on the order of 150 mm. Soot samples were collected along the centerline, at heights corresponding to the maximum primary particle diameter (H = 50 mm), the end of active soot oxidation (H = 110 mm), and past the luminous tip (H = 210 mm). Collection along the centerline of the laminar flames assured that a common streamline was sampled. Fig. 1 shows an image of OH fluorescence and elastic soot scattering in this flame, with the lower two sampling heights indicated.

Flame 2 is a 6-cm diameter ethylene flame stabilized on a McKenna burner with no forced air coflow. It is a buoyant, unsteady, smoking diffusion flame. Soot samples were collected along the flame centerline at a height of 70 mm (nominally at mid-height of the flame) and also downstream of the active combustion zone (in the post-flame region).

Flame 3 is a 5-m diameter JP-8 pool fire; a photograph of which is shown as Fig. 2. The soot samples from this fire were collected in the active flaming region

Table 1
Flame locations sampled with TEM grids

Flame	Fuel	Burner diameter/flow characteristics	Sample locations	Heights sampled
1	Ethylene	1.1 cm/steady laminar	Centerline	H = 50 mm H = 110 mm H = 210 mm
2	Ethylene	6 cm/unsteady laminar	Centerline	H = 70 mm Post-flame
3	JP-8	5 m/turbulent	0.8 m from centerline	H = 1.2 m

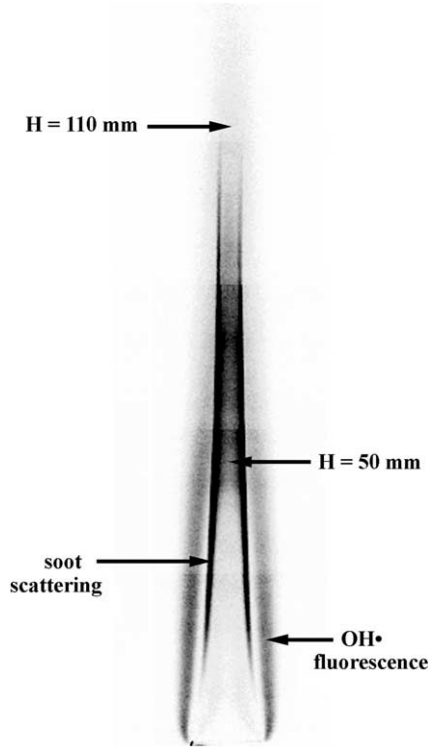

Fig. 1. Stacked planar images of OH· laser-induced fluorescence (on the outer edge of the flame) and elastic soot scattering (inside of the OH· layer) from Flame 1 [47].

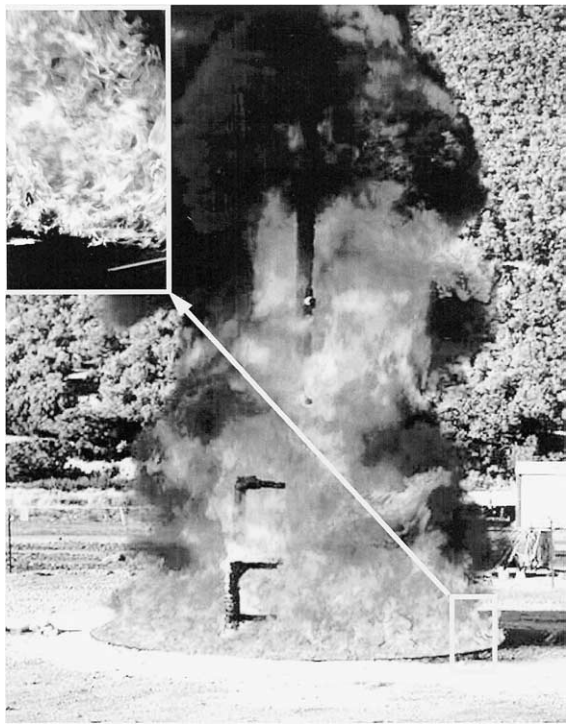

Fig. 2. Photograph of Flame 3, a 5-m JP-8 pool fire at Sandia's Lurance Canyon Burn Site [42]. The inset shows a close-up of the flame structure at the base of the pool fire. (Courtesy of The Combustion Institute.)

of the fire, somewhat off of the fire centerline. Conventional TEM analysis of the grids collected from this fire and from a 1-m diameter JP-8 pool fire has been previously reported in Ref. [42].

HRTEM in lattice fringe mode was performed on the collected soot samples using a Phillips CM30 microscope operating at 300 kV, with a point-to-point resolution of 0.18 nm. Photographic images were collected for representative soot particles and subsequently scanned into a computer for additional digital analysis. Five to seven HRTEM images were collected for each flame sampling position.

In addition to qualitative, visual analysis of the collected HRTEM images, digital analysis of the carbon ordering was conducted using image-processing software. The Semper™ software package, with the custom modifications previously reported by Palotás et al. [10], was used for this purpose. A sample of an HRTEM image and its corresponding carbon fringe image are shown as Fig. 3. Once this fringe image pattern has been extracted, a variety of parameters characterizing the turbostratic carbon may be statistically determined, such as fringe length, fringe circularity/tortuosity, fringe pattern/orientation, fractional coverage, and the graphitic layer interplanar spacing, d_{002}. For the evaluation of the degree of graphitization of carbonaceous materials, the characteristic interplanar spacing has been most commonly used [48]. In many cases, a reduction in d_{002} correlates with growth in the size of the ordered crystallite (both in the graphitic basal plane and perpendicular to it). Therefore, it is often possible to use fringe length as a relative indicator of the degree of graphitization, but the use of interplanar spacing provides a more absolute indication, as it is not constrained by the initial ordering of crystallites within the carbonaceous material.

3. Results

Examples of low-resolution TEM images of the soot collected from Flame 1 at heights of 110 mm and 210 mm are shown in Fig. 4. Detailed examination of these images shows that the soot primary particle size decreases with height above 50 mm. This trend of decreasing primary particle size with increasing height along the flame centerline, even as the soot volume fraction is increasing, has been consistently seen by others probing similar flames [49–51] and is not understood. The micrographs also show that the degree of soot

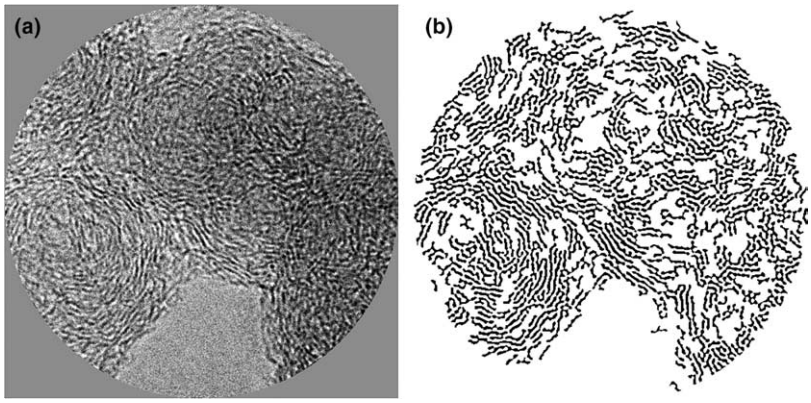

Fig. 3. Circular section of soot HRTEM image (left) and corresponding extracted carbon fringe image pattern (right).

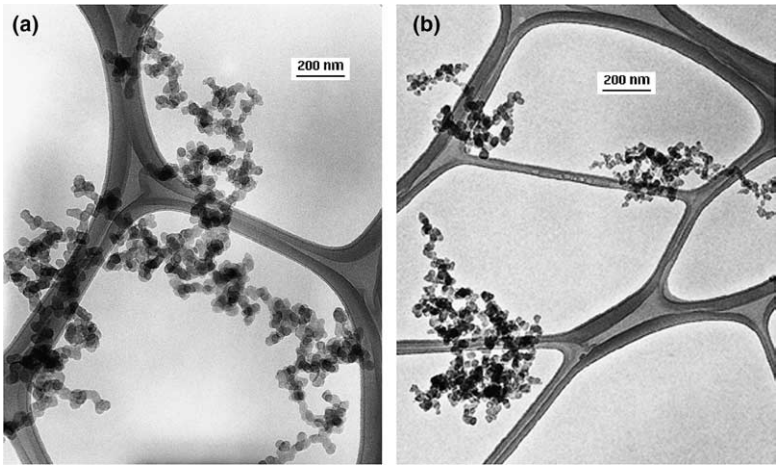

Fig. 4. TEM images on lacey grids of soot collected at $H = 110$ mm (left image) and at $H = 210$ mm (right image) from Flame 1. The magnification is 50,000×.

agglomeration increases with increasing height along the streamline, as expected.

The soot collected at a height of 70 mm in Flame 2 appears to have been newly formed and consists of relatively small agglomerates with an amorphous coating that is present on both the soot aggregates and the TEM grid itself. Upon being exposed to the high-power electron beam used for high-resolution imaging, the amorphous material that had deposited on the grid showed fluidity and covered any deposited soot aggregates (over the course of tens of seconds), preventing effective high-resolution imaging of the soot. An example of such a sequence of events is shown as Fig. 5. It is unclear from the imaging record whether the soot itself dissociated under the high-power electron beam or if the blurring effect in the images resulted entirely from the flow of material originally deposited on the grid surfaces. Others have noted that electron-beam irradiation of carbon forms, while performing HRTEM, heats the samples and can lead to significant structural rearrangements, depending on the intensity and duration of the exposure [52–54]. The samples collected from $H = 50$ mm and $H = 110$ mm in Flame 1 also showed a minor amount of amorphous material coating on both the soot aggregates and the grid surfaces. However, in contrast to the midflame sample from Flame 2, the grid-deposited amorphous material did not show fluidity during HRTEM imaging of any of the soot samples from Flame 1.

Samples of HRTEM images from all 3 flames are presented in Fig. 6. All of the samples show the characteristic "onion" shape of turbostratic graphitic ordering (i.e., concentrically oriented graphene layers) that has been generally found for soot. In some instances the outer layers of the primary particles are ordered about a relatively unordered center, whereas in other cases

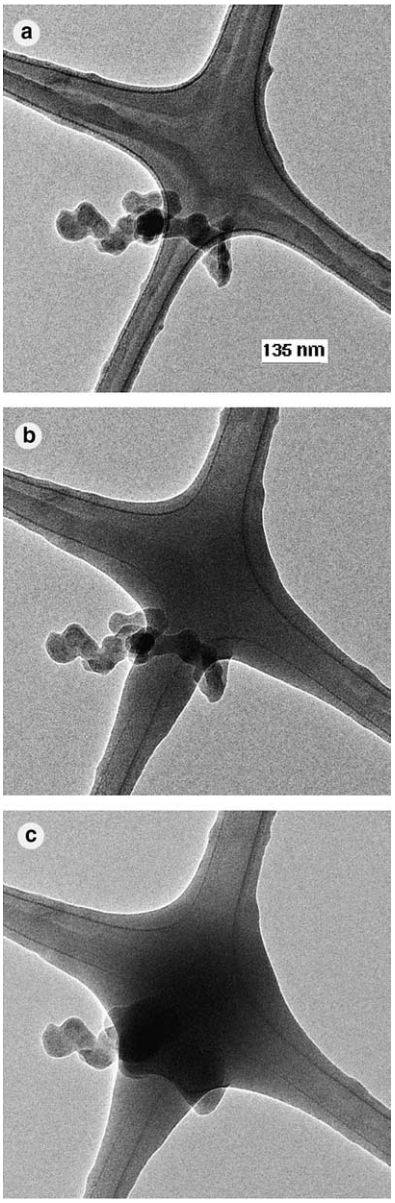

Fig. 5. Series of consecutive TEM images (top to bottom) at a magnification of 70,000× showing the effect of exposure of soot and grid deposits from $H = 70$ mm in Flame 2 to a high-power electron beam. Each image was collected approximately 30 s subsequent to the previous image.

there are several centers of ordering within a given primary particle or within joined primary particles. Qualitatively, when viewing all of the collected HRTEM images, there appears to be a progression in the extent of graphitic ordering in these images as the height increases along the centerline of Flame 1. As shown in Fig. 7, the soot that had recently formed at the first centerline sampling height ($H = 50$ mm), experienced a temperature of 1500–1600 K for 25 ms before reaching the second sampling height, and then experienced a longer period (35 ms) over a lower temperature range of 1000–1500 K before reaching the final sampling height. Therefore, an increase in graphitic ordering of the soot may be anticipated as a consequence of thermal annealing along the flame centerline.

In order to quantify the visually apparent trend of increased carbon ordering and to determine the relative graphitization of the soot in the different flames, quantitative image analysis of the HRTEM images was performed, as previously described. Table 2 shows the results for the analysis of graphitic layer interplanar spacing in all of the analyzed soot samples. Both the mean values of the interplanar spacing and the calculated standard deviations in the distribution of individual paracrystalline layer spacings are listed. As previously found by Palotás et al. [3,4], the standard deviation in the interplanar spacing is relatively large, apparently reflecting the inherently wide, multimodal distribution of interplanar spacings in turbostratic carbons and even graphitized carbons. As discussed in Refs. [3,4], a variety of discrete interplanar spacing values between 3.38 and 3.87 Å have been measured in these forms of carbon using both HRTEM and X-ray diffraction. Furthermore, previous digital analysis of HRTEM images of a highly graphitized carbon black yielded a standard deviation in the interlayer spacing of 0.07 Å [4], so this should be considered a practical lower limit of this quantity.

4. Discussion

The majority of the measurements of mean interplanar spacing of graphitic layers in combustion-derived soot have yielded values of between 3.4 and 3.6 Å [2], comparable to the range of interplanar spacing that has been measured via XRD for carbon black [56]. By comparison, the interlayer spacing is 3.35 Å in pure graphite. The values for mean d_{002} determined by HRTEM for the soot in the current investigation range from 3.47 to 3.57 Å and are therefore consistent with these previous findings. Similarly, the range of standard deviation in d_{002} found for the soot in the current investigation is similar to that found previously for carbon black and other partially ordered carbons when using the same analytical approach [4].

The trend in the mean interplanar spacing for the steady, laminar flame offers weak evidence of densification of the graphitic layers as the soot is convected along the flame centerline near its peak temperature of ~1600 K between heights of 50 mm and 110 mm. Once the combustion of hydrocarbon fragments, H_2, and CO has concluded (at a height around 110 mm), and the gas temperature begins to drop substantially, no fur-

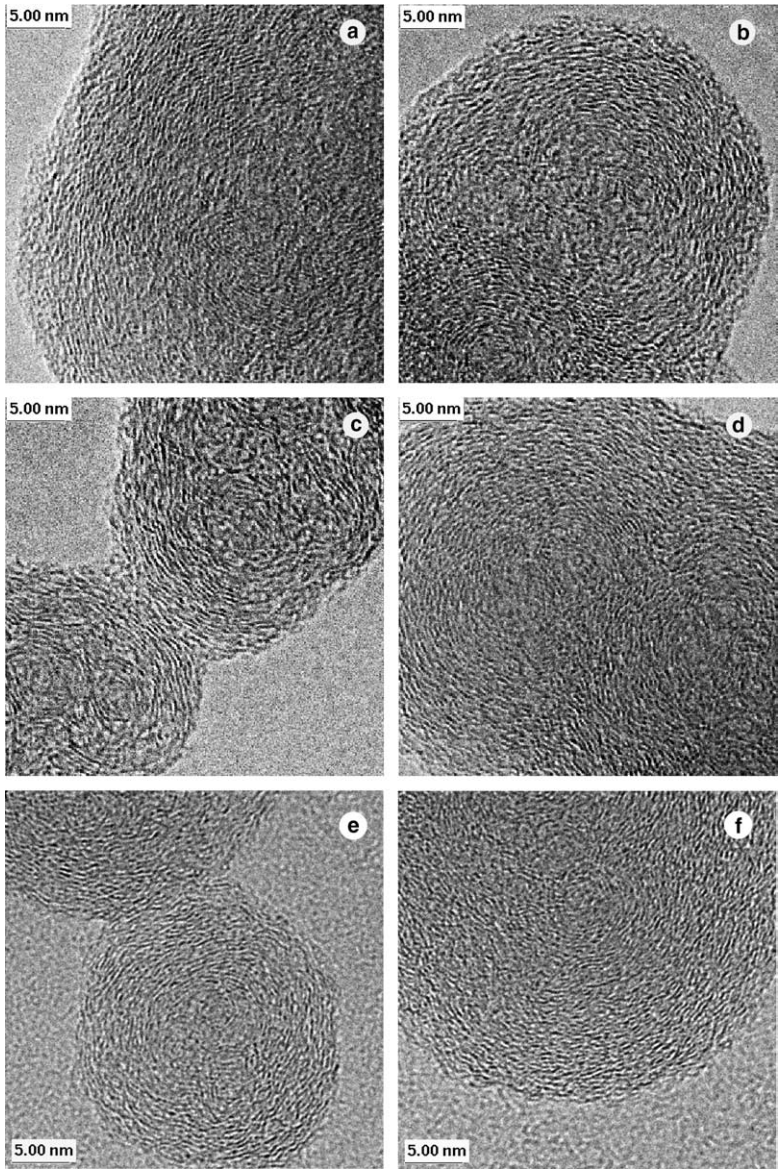

Fig. 6. High-resolution TEM images (magnification of 1,800,000×) from different sampling locations and flames: (a) Flame 1, $H = 50$ mm; (b) Flame 1, $H = 110$ mm; (c) Flame 1, $H = 210$ mm; (d) Flame 2, post-flame; and (e) and (f) Flame 3.

ther increase in turbostratic ordering occurs. The high activation energy associated with the annealing of semi-ordered carbon (generally estimated as over 200 kJ/mol [57,58]) results in a strong sensitivity of annealing to temperature variations, consistent with the trend in soot annealing observed here.

The soot samples from the post-flame region of the unsteady ethylene flame and from within the JP-8 pool fire both show slightly larger mean interplanar spacing than is present for any of the sampled heights along the centerline of the steady laminar flame. This result may be indicative of the influence of the lower temperatures expected in the soot formation region in the larger, unsteady laminar flame and in the JP-8 pool fire, or it may be an artifact of the limited number of soot particles analyzed and the wide distribution of interplanar spacings at any given sampling location. The standard deviation of the interlayer spacing might be expected to be larger for the soot sampled from the unsteady flame and from the turbulent pool fire, in particular, but no such trend is evident. A possible explanation is that the TEM grid sampling time scales may be short in comparison to the characteristic vortex turnover timescales in both of these environments, in which case no

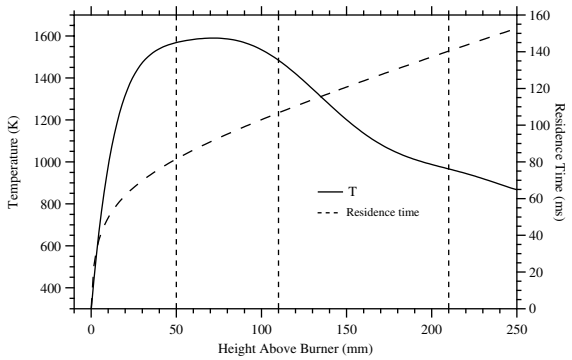

Fig. 7. Temperature and residence time profiles along the centerline of Flame 1, as given in Ref. [55]. Dashed, vertical lines indicate the heights at which soot samples were collected on TEM grids.

extraordinary variation in the interlayer spacing would be expected.

Vaglieco et al. [59] pointed out that the available data on the effect of thermal annealing on semi-ordered carbons, including amorphous carbon films and coal vitrinite, show a modest decrease in the real component of the refractive index and a strong increase in the imaginary component. In particular, thermal annealing of an amorphous carbon film has been shown to increase the imaginary portion of its index of refraction at 500 nm from 0.28 to 0.98 [60]. Some studies have begun to link measured optical properties with experimental indications of the ratio of sp^2 to sp^3 bonding in carbon black [13,40], but no measurements have been reported of optical properties or bonding ratios of soot or carbon black as a function of interlayer spacing. Consequently, the results of the current study suggest that an increase in the optical absorptivity of post-inception, agglomerating soot may occur during the course of its growth and oxidation in laminar diffusion flames (and probably in some turbulent diffusion flames). However, the small differences in mean interplanar spacing which are seen, together with the wide distributions of spacing present in each soot sample, suggest that the resultant optical property variations, if they occur at all, are quite small.

This conclusion is consistent with measurements of the dimensionless extinction coefficient of soot emitted from laminar and turbulent flames of a wide variety of fuels, both gaseous and liquid, which show only a small variability at visible wavelengths, at least part of which is attributable to differences in scattering contributions and shielding effects [61–63]. Recent measurements of the dimensionless extinction coefficient of soot sampled from *within* JP-8 pool fires [64] also show values within the range of 8–10 previously measured for the post-flame soot. These results are in agreement with the similarity of soot carbon interlayer spacings found in the present study. Taken together, the recent extinction coefficient measurements and the current HRTEM analysis suggest that once solid, aggregating primary particles are formed, the soot optical properties (from a material perspective) are essentially fixed. This is a convenient and important finding, both for interpretation of optical extinction measurements of soot concentration and for predictions of radiant absorption or emission from soot. However, this finding conflicts with the wide variety of soot refractive index values reported in the literature [65]. It is important, however, to note that most of the reported refractive indices provide imaginary components that are too low in comparison with the measured dimensionless extinction coefficients (even when taking into account the scattering contribution from soot aggregates [66]). The high variability in the reported refractive indices and their low imaginary component suggests that many of these studies have included contributions from condensed tars and/or precursor particles, in addition to solid soot particles.

5. Conclusions

Results from an HRTEM study of soot microstructure evolution along a streamline in a laminar ethylene/air diffusion flame are reported, and show a minor decrease in mean graphitic interplanar spacing as the soot moves through the high-temperature growth region. Comparison with soot collected in the post-flame zone of a larger, unsteady ethylene/air diffusion flame and from the active flaming-region of a large JP-8 pool fire reveals slightly greater interplanar spacing in the larger flames, perhaps reflecting lower temperatures in the soot formation regions of these flames. In all cases, wide

Table 2
Graphitic layer interplanar spacing in collected soots

Flame	Fuel	Burner diameter/flow characteristics	Sample location	Mean d_{002} (Å)	SD d_{002} (Å)
1	Ethylene	1.1 cm/steady laminar	H = 50 mm	3.52	0.14
			H = 110 mm	3.48	0.15
			H = 210 mm	3.47	0.10
2	Ethylene	6 cm/unsteady laminar	Post-flame	3.57	0.12
3	JP-8	5 m/turbulent	H = 1.2 m	3.55	0.14

distributions of interplanar spacing are apparent for each soot sample set. These results suggest that the optical absorptivity of the soot is similar for all of the interrogated flames, and increases a small amount, if at all, in the upper regions of the laminar diffusion flame. This is a convenient and important finding, both for interpretation of optical extinction measurements of soot concentration and for predictions of radiant absorption or emission from soot.

Acknowledgements

This research was partially supported through a Laboratory Directed Research and Development (LDRD) project at Sandia National Labs, as well as by the grants of the Hungarian State Eötvös Fellowship and project FKFP 0083/2001. Jill Suo-Anttila (nee Williams) of Sandia graciously provided the TEM grid samples from the JP-8 pool fire and Thomas Headley, also of Sandia, is gratefully acknowledged for his assistance in performing the HRTEM. Sandia is operated by the Sandia Corporation, a Lockheed Martin Company, for the US DOE under contract DE-AC04-94-AL85000.

References

[1] R.A. Dobbins, The early soot particle formation in hydrocarbon flames, in: F.L. Dryer, R.F. Sawyer (Eds.), Physical and Chemical Aspects of Combustion: a Tribute to Irvin Glassman, Gordon and Breach Science Publishers, The Netherlands, 1997, pp. 107–133.

[2] H.X. Chen, R.A. Dobbins, Crystallogenesis of particles formed in hydrocarbon combustion, Combust. Sci. Tech. 159 (2000) 109–128.

[3] Á.B. Palotás, L.C. Rainey, A.F. Sarofim, J.B. Vander Sande, R.C. Flagan, Where did that soot come from? Chemtech 28 (1998) 24–30.

[4] Á.B. Palotás, L.C. Rainey, A.F. Sarofim, J.B. Vander Sande, P. Ciambelli, Effect of oxidation on the microstructure of carbon blacks, Energy Fuels 10 (1996) 254–259.

[5] K. Das Chowdhury, J.B. Howard, J.B. Vander Sande, Fullerenic nanostructures in flames, J. Mat. Res. 11 (1996) 341–347.

[6] W.J. Grieco, J.B. Howard, L.C. Rainey, J.B. Vander Sande, Fullerenic carbon in combustion-generated soot, Carbon 38 (2000) 597–614.

[7] P. Hebgen, A. Goel, J.B. Howard, L.C. Rainey, J.B. Vander Sande, Synthesis of fullerenes and fullerenic nanostructures in a low-pressure benzene/oxygen diffusion flame, Proc. Comb. Instit. 28 (2000) 1397–1404.

[8] A. Goel, P. Hebgen, J.B. Vander Sande, J.B. Howard, Combustion synthesis of fullerenes and fullerenic nanostructures, Carbon 40 (2002) 177–182.

[9] K.A. Davis, R.H. Hurt, N.Y.C. Yang, T.J. Headley, Evolution of char chemistry, crystallinity, and ultrafine structure during pulverized-coal combustion, Comb. Flame 100 (1995) 31–40.

[10] Á.B. Palotás, L.C. Rainey, C.J. Feldermann, A.F. Sarofim, J.B. Vander Sande, Soot morphology: An application of image analysis in high-resolution transmission electron microscopy, Micros. Res. Tech. 33 (1996) 266–278.

[11] A. Sharma, T. Kyotani, A. Tomita, A new quantitative approach for microstructural analysis of coal char using HRTEM images, Fuel 78 (1999) 1203–1212.

[12] H.-S. Shim, R.H. Hurt, N.Y.C. Yang, A methodology for analysis of 002 lattice fringe images and its application to combustion-derived carbons, Carbon 38 (2000) 29–45.

[13] Ch. Jäger, T. Henning, R. Schlögl, O. Spillecke, Spectral properties of carbon black, J. Non-Cryst. Solids 258 (1999) 161–179.

[14] C.M. Sorensen, Light scattering by fractal aggregates: a review, Aerosol Sci. Tech. 35 (2001) 648–687.

[15] R. Jullien, R. Botet, Aggregation and Fractal Agglomerates, World Scientific Publishing Co., Singapore, 1987.

[16] C.M. Megaridis, R.A. Dobbins, Morphological description of flame-generated materials, Combust. Sci. Tech. 71 (1990) 95–109.

[17] G.M. Faeth, Ü.Ö. Köylu, Soot morphology and optical properties in nonpremixed turbulent flame environments, Combust. Sci. Tech. 108 (1995) 207–229.

[18] T.L. Farias, M.G. Carvalho, Ü.Ö. Köylu, G.M. Faeth, Computational evaluation of approximate Rayleigh–Debye–Gans/fractal-aggregate theory for the absorption and scattering properties of soot, J. Heat Transfer 117 (1995) 152–159.

[19] T.L. Farias, Ü.Ö. Köylu, M.G. Carvalho, Effects of polydispersity of aggregates and primary particles on radiative properties of simulated soot, J. Quant. Spectr. Rad. Trans. 55 (1996) 357–371.

[20] T.L. Farias, Ü.Ö. Köylu, M.G. Carvalho, Range of validity of the Rayleigh–Debye–Gans theory for optics of fractal aggregates, Appl. Opt. 35 (1996) 6560–6567.

[21] C. Oh, C.M. Sorensen, The effect of overlap between monomers on the determination of fractal cluster morphology, J. Colloid Interface Sci. 193 (1997) 17–25.

[22] G.W. Mulholland, C.F. Bohren, K.A. Fuller, Light-scattering by agglomerates—coupled electric and magnetic dipole method, Langmuir 10 (1994) 2533–2546.

[23] G.W. Mulholland, R.D. Mountain, Coupled dipole calculation of extinction coefficient and polarization ratio for smoke agglomerates, Comb. Flame 119 (1999) 56–68.

[24] Ü.Ö. Köylu, G.M. Faeth, Optical properties of overfire soot in buoyant turbulent diffusion flames at long residence times, J. Heat Transfer 116 (1994) 152–159.

[25] J.Y. Zhu, M.Y. Choi, G.W. Mulholland, L.A. Gritzo, Soot scattering measurements in the visible and near-infrared spectrum, Proc. Comb. Instit. 28 (2000) 439–446.

[26] S.S. Krishnan, K.-C. Lin, G.M. Faeth, Extinction and scattering properties of soot emitted from buoyant turbulent diffusion flames, J. Heat Transfer 123 (2001) 331–339.

[27] A. Becker, Ann. Physik 28 (1909) 1017.

[28] R.C. Millikan, Sizes optical properties and temperatures of soot particles, in: Temperature: Its Measurement and Control in Science and Industry, vol. 3, Reinhold Publishing, New York, 1962, pp. 497–507.

[29] S.C. Lee, C.L. Tien, Optical constants of soot in hydrocarbon flames, Proc. Comb. Instit. 18 (1981) 1159–1166.
[30] T.T. Charalampopoulos, H. Chang, B. Stagg, The effects of temperature and composition on the complex refractive-index of flame soot, Fuel 68 (1989) 1173–1179.
[31] B.J. Stagg, T.T. Charalampopoulos, Refractive-indexes of pyrolytic-graphite, amorphous carbon and flame soot in the temperature-range 25 to 600 °C, Comb. Flame 94 (1993) 381–396.
[32] R.A. Dobbins, R.A. Fletcher, H.-C. Chang, The evolution of soot precursor particles in a diffusion flame, Comb. Flame 115 (1998) 285–298.
[33] B.L. Wersborg, L.K. Fox, J.B. Howard, Soot concentration and absorption-coefficient in a low-pressure flame, Comb. Flame 24 (1975) 1–10.
[34] U. Bonne, H.Gg. Wagner, Untersuchung des reaktionsablaufs in fetten kohlenwasserstoff-sauerstoff-flammen 3. Optische untersuchungen an russenden flammen, Ber. Bunsenges. Physik Chem. 69 (1965) 35.
[35] A. D'Alessio, F. Beretta, C. Venitozzi, Optical investigations on soot forming methane-oxygen flames, Combust. Sci. Tech. 5 (1972) 263–272.
[36] R.A. Dobbins, R.A. Fletcher, W. Lu, Laser microprobe analysis of soot precursor particles and carbonaceous soot, Comb. Flame 100 (1995) 301–309.
[37] P. Minutolo, G. Gambi, A. D'Alessio, The optical band gap model in the interpretation of the UV–visible absorption spectra of rich premixed flames, Proc. Comb. Instit. 26 (1997) 951–957.
[38] F.W. Smith, Optical constants of a hydrogenated amorphous carbon film, J. Appl. Phys. 55 (1984) 764–771.
[39] W.W. Duley, S. Seahra, Graphite, polycyclic aromatic hydrocarbons, and the 2175 A extinction feature, Astrophys. J. 507 (1998) 874–888.
[40] B. Michel, Th. Henning, C. Jäger, U. Kreibig, Optical extinction by spherical carbonaceous particles, Carbon 37 (1999) 391–400.
[41] R.A. Dobbins, C.M. Megaridis, Morphology of flame-generated soot as determined by thermophoretic sampling, Langmuir 3 (1987) 254–259.
[42] J.M. Williams, L.A. Gritzo, In situ sampling and transmission electron microscope analysis of soot in the flame zone of large pool fires, Proc. Comb. Instit. 27 (1998) 2707–2714.
[43] R.J. Santoro, H.G. Semerjian, R.A. Dobbins, Soot particle measurements in diffusion flames, Comb. Flame 51 (1983) 203–218.
[44] R.J. Santoro, H.G. Semerjian, Soot formation in diffusion flames: flow rate, fuel species and temperature effects, Proc. Comb. Instit. 20 (1984) 997–1006.
[45] R.J. Santoro, T.T. Yeh, J.J. Horvath, H.G. Semerjian, The transport and growth of soot particles in laminar diffusion flames, Combust. Sci. Tech. 53 (1987) 89–115.
[46] C.M. Megaridis, R.A. Dobbins, Comparison of soot growth and oxidation in smoking and non-smoking ethylene diffusion flames, Combust. Sci. Tech. 66 (1989) 1–16.
[47] C.R. Shaddix, K.C. Smyth, unpublished data.
[48] K. Kinoshita, Carbon: Electrochemical and Physicochemical Properties, John Wiley & Sons, New York, 1988, p. 60.
[49] P.B. Sunderland, Ü.Ö. Köylü, G.M. Faeth, Soot formation in weakly buoyant acetylene-fueled laminar jet diffusion flames burning in air, Comb. Flame 100 (1995) 310–322.
[50] P.B. Sunderland, G.M. Faeth, Soot formation in hydrocarbon/air laminar jet diffusion flames, Comb. Flame 105 (1996) 132–146.
[51] F. Xu, G.M. Faeth, Soot formation in laminar acetylene/air diffusion flames at atmospheric pressure, Comb. Flame 125 (2001) 804–819.
[52] D. Ugarte, Curling and closure of graphitic networks under electron-beam irradiation, Nature 359 (1992) 707–709.
[53] M. Miki-Yoshida, R. Castillo, S. Ramos, L. Rendón, S. Tehuacanero, B.S. Zou, M. José-Yacamán, High resolution electron microscopy studies in carbon soots, Carbon 32 (1994) 231–246.
[54] D. Ugarte, Onion-like graphitic particles, Carbon 33 (1995) 989–993.
[55] T.F. Richardson, R.J. Santoro, Private communication, 1993.
[56] A.E. Austin, Crystal structure properties of carbon blacks, in: Proceedings of the 3rd Conference on Carbon, University of Buffalo, New York, 1958, pp. 389–394.
[57] A. Zolin, A. Jensen, K. Dam-Johansen, Kinetic analysis of char thermal deactivation, Proc. Comb. Instit. 28 (2000) 2181–2188.
[58] N.V. Russell, J.R. Gibbins, C.K. Man, J. Williamson, Coal char thermal deactivation under pulverized fuel combustion conditions, Energy Fuels 14 (2000) 883–888.
[59] B.M. Vaglieco, F. Beretta, A. D'Alessio, In situ evaluation of the soot refractive-index in the UV–visible from the measurement of the scattering and extinction coefficients in rich flames, Comb. Flame 79 (1990) 259–271.
[60] D.R. McKenzie, R.C. McPhedran, N. Savvides, L.C. Botten, Properties and structure of amorphous hydrogenated carbon films, Phil. Mag. B 48 (1983) 341–364.
[61] G.W. Mulholland, M.Y. Choi, Measurement of the mass specific extinction coefficient for acetylene and ethane smoke using the large agglomerate optics facility, Proc. Comb. Instit. 27 (1998) 1515–1522.
[62] S.S. Krishnan, K.-C. Lin, G.M. Faeth, Optical properties in the visible of overfire soot in large buoyant turbulent diffusion flames, J. Heat Transfer 122 (2000) 517–524.
[63] J. Zhu, A. Irrera, M.Y. Choi, G.W. Mulholland, L. Gritzo, J. Suo-Anttila, Measuement of light extinction constant of JP-8 soot in the visible and near-infrared spectrum, Int. J. Heat Mass Transfer 47 (2004) 3643–3648.
[64] K.A. Jensen, J.M. Suo-Anttila, L.G. Blevins, Measurement of soot morphology, chemistry, and optical properties in the visible and near-infrared spectrum in the flame zone and overfire region of large JP-8 pool fires, Comb. Flame, submitted for publication.
[65] K.C. Smyth, C.R. Shaddix, The elusive history of $m = 1.57–0.56i$ for the refractive index of soot, Comb. Flame 107 (1996) 314–320.
[66] J. Zhu, M.Y. Choi, G.W. Mulholland, S.L. Manzello, L.A. Gritzo, Measurement of visible and near-IR optical properties of soot produced from laminar flames, Proc. Comb. Instit. 29 (2003) 2367–2374.